Supplemental Information

Nintedanib is a highly effective therapeutic for neuroendocrine carcinoma of the pancreas (PNET) in the Rip1Tag2 transgenic mouse model

Ruben Bill, Ernesta Fagiani, Adrian Zumsteg, Helena Antoniadis, David Johansson, Simon Haefliger, Imke Albrecht, Frank Hilberg, and Gerhard Christofori

Supplemental Material and Methods

Immunohistochemistry and metastasis analysis

For the detection of liver and lymph node metastases, 5μm thick PFA-fixed paraffin-embedded liver and pancreas sections were deparaffinized and antigen-retrieval was performed in a pressure cooker (PrestigeMedical) in 10mM Na-Citrate buffer (pH 6.0). IHC stainings were conducted using Dako EnVision plus kit (Dako) according to the manufacturer's advices. Metastatic tumor cells were indentified by staining with an antibody against SV40 Large-T antigen (rabbit polyclonal IgG, Santa Cruz, sc-20800, 1:50 dilution) and were counterstained with hematoxylin before mounting with Cytoseal™ XYL (Thermo scientific). 9 serial liver sections per mouse were analyzed with each section 75μm apart. The whole liver was embedded to ensure a comprehensive analysis of all liver lobes. Intravascular metastases were excluded. SV40 Large T antigen-positive single tumor cells localized in the liver parenchyme were included in the analysis. For the detection of pancreatic lymph node metastases, 1 section per lymph node was analyzed.

Double-strand DNA breaks associated with apoptotic and non-apoptotic cell death were visualized using a TUNEL assay (*In Situ* Cell Death Detection Kit, POD; Roche) according to the manufacturer`s recommendations, using Proteinase K pretreatment. The staining was developed with 3-amino-9-ethylcarbazole (AEC, Vector Labs) and

briefly counterstained with hematoxylin. Light microscopy images were obtained with an AxioVert microscope (Leica Microsystems) or with a Zeiss Axio Observer (Zeiss).

Immunofluorescence

8μm thick cryosections were dried for 30 minutes at room temperature (RT), 5 minutes rehydrated in PBS, permeabilized in PBS/0.1% Triton X-100 during 20 minutes and blocked with PBS/5% normal goat serum (NGS; Sigma). As an exception, cleaved Caspase-3 (cCasp3) stainings were blocked with PBS/20%NGS. All primary antibodies were diluted in PBS/5%NGS. The following antibodies and dilutions were used: rat anti-CD31 (BD Pharmingen, 550274, 1:50), rabbit anti-NG2 (Chemicon, AB5320, 1:100), guinea-pig anti-insulin (Dako, A0564, 1:200), rabbit anti-α-amylase (Sigma, A8273, 1:100), rabbit anti-cleaved Caspase-3 (Cell Signaling, 9664, 1:50), rabbit anti-phospho Histone H3 (Millipore, 06-570, 1:200), rabbit anti-LYVE-1 (RELIATech, 103-PA50S/0412P02-2, 1:200). Positive staining was visualized by incubating the specimen during 1 hour with secondary antibodies against the respective species of the corresponding first antibody, labeled with either Alexa488, Alexa568 or Alexa633 (Molecular probes; 1:200 in PBS/5%NGS). Nuclei were stained with DAPI (Sigma) and slides were mounted with Dako mounting medium (Dako). Fluorescence images were acquired with a Leica DMI 4000 or a Nikon Diaphot 300 microscope.

In Figure S4A, IF staining against CD31 was performed on 5μm thick PFA-fixed paraffin-embedded pancreata (PFFPE). The tissue was deparaffinized, rehydrated in PBS and antigen retrieval was performed with PBS/0.1% proteinase K (Fluka) for 20 minutes at 37°C. Endogenous peroxidase was quenched with 3% H_2O_2, washed in PBS and blocked with PBS/5% NGS for 30 minutes at RT. Primary antibody incubation (rat anti-CD31; Bachem, T-2001, 1:50) and the subsequent staining procedure was performed as described for immunofluorescence staining.

Supplemental Figure Legends

Supplemental Figure S1: Nintedanib increases tumor cell apoptosis yet does not affect tumor cell proliferation.

(A) Representative microphotographs of hematoxylin and eosin stained sections of the various stages of tumor progression in Rip1Tag2 transgenic mice. Shown are sections of non-invasive adenoma with smooth tumor borders (Adenoma), microinvasive carcinoma with 1-2 invasive protrusions into the surrounding exocrine pancreas (dashed line) (IC1), and macro-invasive (dashed line; i) and anaplastic carcinoma (ii) (IC2). Scale bar, 100µm.

(B) The number of cells with double-strand DNA breaks indicating apoptotic and non-apoptotic cell death was analyzed by Tunel assay. Representative microphotographs are shown, and the number of Tunel-positive cells per area and field of view was determined as mean ± SEM. N=2 mice per group. Scale bar, 50µm. *, $P < 0.05$.

(C) The number of dividing cells was determined by immunofluorescence staining of phospho-histone 3 (pH3). Representative microphotographs are shown, and pH3-positive cells per area and field of view were counted and displayed in a bar graph as mean ± SEM. Vehicle: n=4 mice, nintedanib: n=7 mice. Scale bar, 100µm. Statistical analysis was performed employing an unpaired Student *t* test (B, C).

(D) Primary insulinoma tumor cells were treated for 4 days with nintedanib *in vitro*. The number of intact cells/well was determined and displayed per nintedanib concentrations. 3 independent experiments in triplicates were performed and shown as mean ±SEM for each nintedanib concentration. Graphical representation was achieved calculating a non-linear regression of the normalized response allowing a variable slope over the logarithmic inhibitor concentration. $IC_{50} = 1.891 \times 10^{-6}$ M.

Supplemental Figure S2: Blood vessels resisting nintedanib-treatment display a mature phenotype and retain their function.

(A, B) Quantification and analysis of the relative localization of $NG2^+$ perivascular cells to $CD31^+$ blood vessels revealed in nintedanib-treated tumors a reduction of total $NG2^+$ perivascular cells per area (A) and an increased percentage of $NG2^+$ perivascular cells not associated with blood vessels (B). Values are displayed as counts per area of each field of view. Statistical analysis was performed using an unpaired Student *t* test; ***, P < 0.001. Vehicle: n=4 mice, nintedanib: n=7 mice.

Supplemental Figure S3: Nintedanib induces hypoxia in a subset of tumors.

(A) Representative immunofluorescence images of pimonidazole-positive area fractions of tumors representing tissue hypoxia. Scale bar, 100µm.

(B, C) Quantification of the percentages of tumors with any signs of hypoxia compared to the total number of tumors per experimental group (B) and of the pimonidazole-positive (red) tumor area fractions of hypoxic tumors (C). Cell nuclei are visualized by DAPI staining (blue). Data are displayed as mean ± SEM. Vehicle: n=6 mice, nintedanib: n=7 mice. P-values were calculated using a Fisher's exact (B) and an unpaired Student *t* test (C); *, P < 0.05.

(**D**) A representative immunofluorescence image of a pimonidazole-positive hypoxic area close to the non-invasive tumor border (dashed line) is shown. Scale bar, 100µm.

Figure S4. Nintedanib, PTK/ZK and sunitinib treatment reduce MVD and tumor volume and do not induce tumor invasiveness

(A, B) A 5-day nintedanib PTK/ZK or sunitinib-treatment was initiated in 9 weeks old Rip1Tag2 mice, and blood microvessel density, as determined by CD31 immunofluorescence staining per field of view (A), and tumor volumes (B) were quantified. N=5 mice per group. P-values were calculated employing an unpaired Student *t* test (A) and a Mann-Whitney *U* test (B) respectively; ***, P < 0.001.

(C) Grading of tumor stages in Rip1Tag2 mice treated for 5 days with nintedanib, PTK/ZK, sunitinib or vehicle control initiated at 9 weeks of age (as described in panels B, C). N=5 mice per group. Fisher`s exact test; *, $P < 0.05$.

Figure S5. Prolonging survival by nintedanib does not increase liver metastasis

Mice were treated with nintedanib or vehicle control open end and euthanized before they succumbed to hypoglycemia or other tumor-related complications (survival trial). Livers were screened for metastasis by immunohistochemical staining for SV40 Large-T antigen. Nine sections per liver were analyzed. Vehicle: n=9 mice, nintedanib: n=8 mice. Statistical analysis was performed employing a Mann-Whitney *U* test.

Figure S6. Nintedanib and sunitinib treatment reduce MVD and tumor volumes.

(A - D) Rip1Tag2 mice were treated with nintedanib for 5 days starting at the age of 11 weeks (A, B) or with sunitinib for 3 weeks starting at the age of 9 weeks (C, D). Tumor microvessel density was determined by CD31 immunofluorescence staining per field of view (A, C), and tumor volumes (B, D) were quantified. N=10 mice per group for (A). (B) pooled data of 5 independent experiments are displayed; vehicle: n=28 mice, nintedanib: n=30 mice. (C, D) control: n=10 mice, sunitinib: n=11 mice. P-values were calculated by unpaired Student *t* test (A, C) or Mann-Whitney *U* test (B, D). *, $P < 0.05$; ***, $P < 0.001$.

Figure S7. PTK/ZK treatment reduces MVD and tumor volume.

(A – D) 9 weeks old Rip1Tag2 mice were treated with PTK/ZK for 3-6 weeks (A, B) or for 5 days starting at the age of 11 weeks (C, D). Tumor microvessel densities were determined by CD31 immunofluorescence staining per area of each field of view and displayed as mean ± SEM (A, C). Tumor volumes are represented in (B) and (D), respectively. (A, B) PEG: N=4 mice, PTK/ZK: N=3-5 mice per group. (C) one

representative experiment is shown. (D) 3 independent experiments were pooled; PEG: N=10 mice, PTK/ZK: N=9 mice. Statistical analysis was performed using an unpaired Student *t* test (A, C) or Mann-Whitney *U* test (B, D). ***, $P < 0.001$.

Supplemental Figure S1

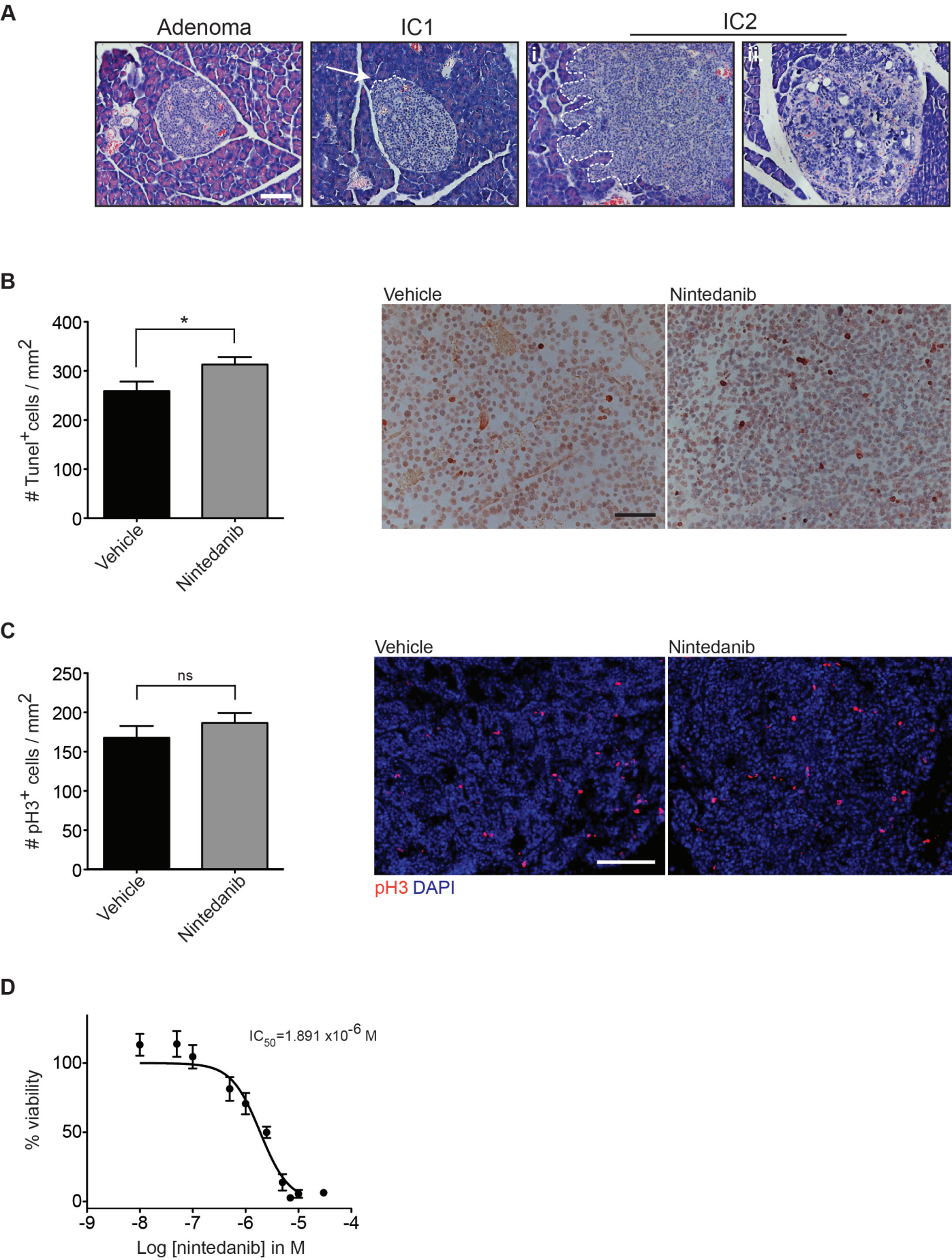

Supplemental Figure S2

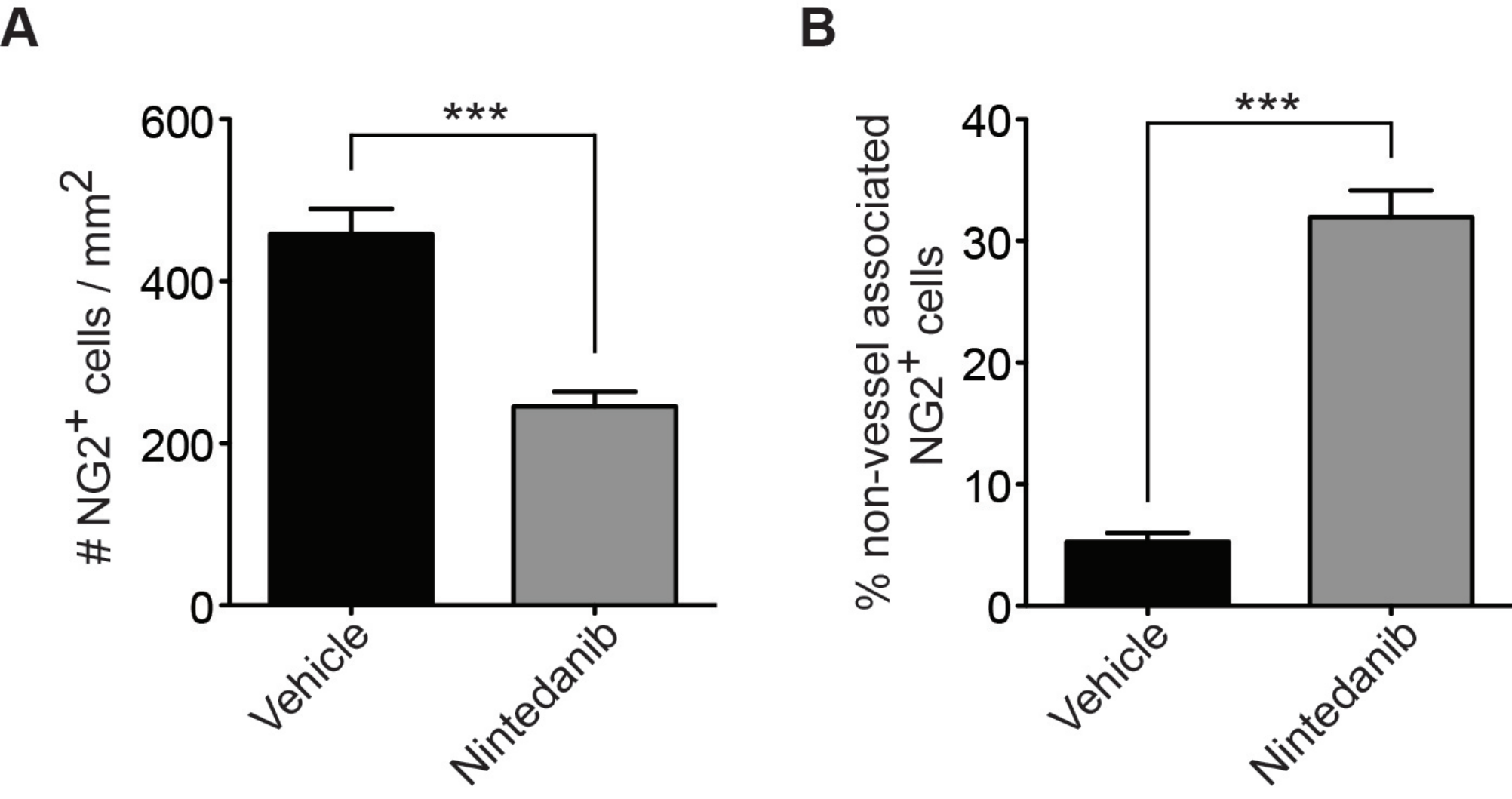

Supplemental Figure S3

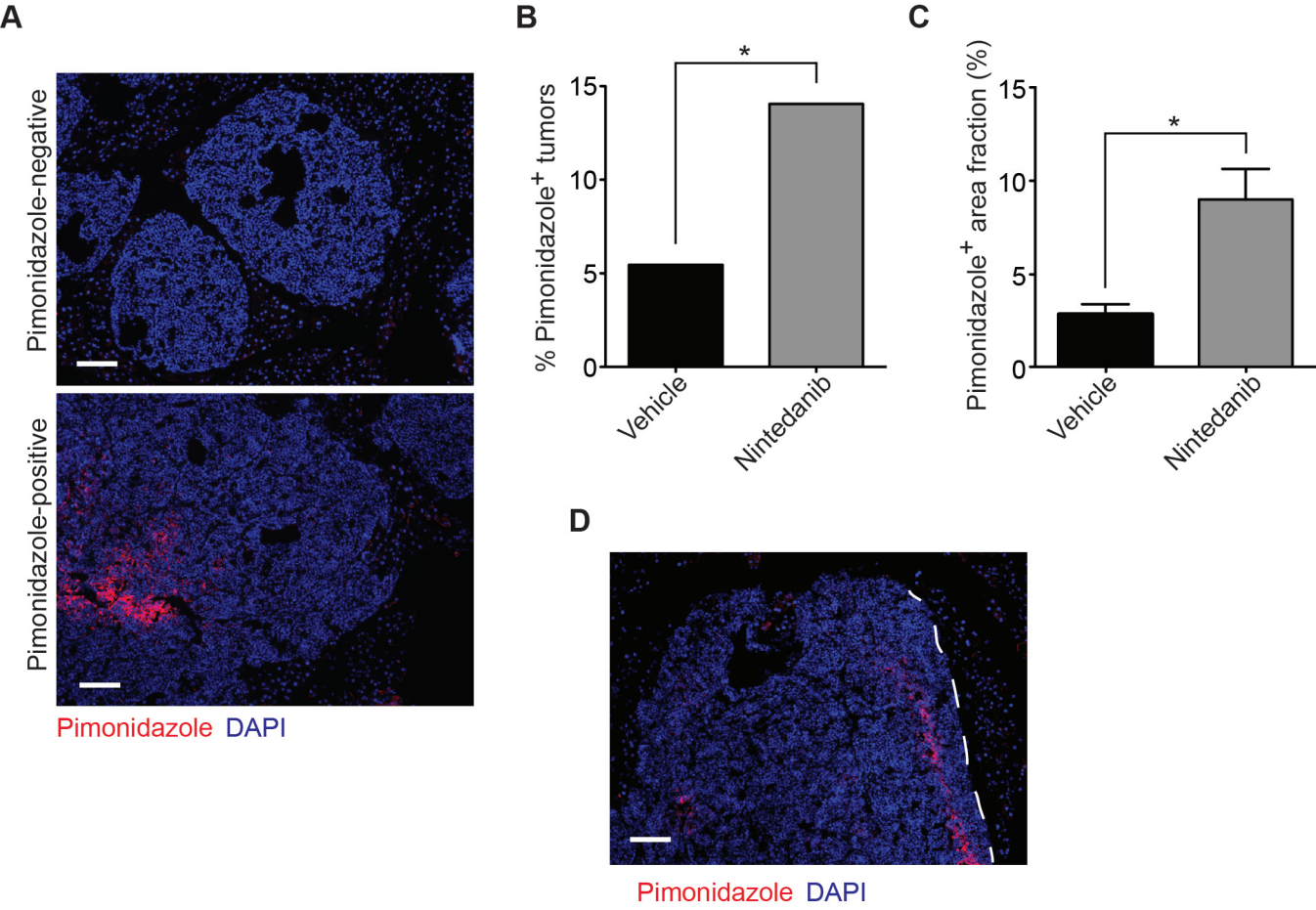

Supplemental Figure S4

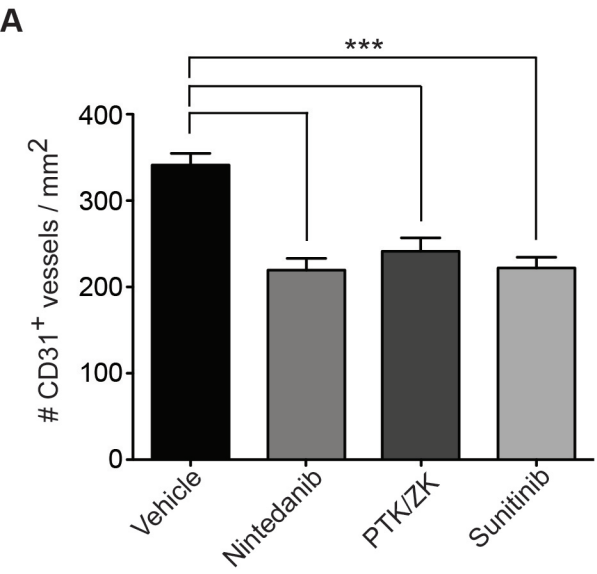

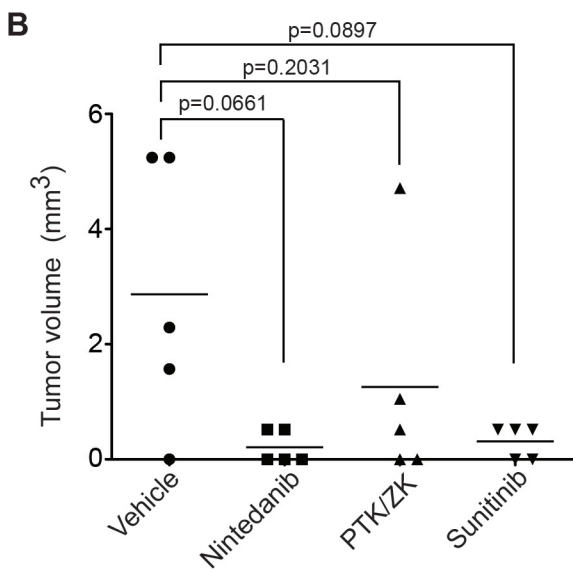

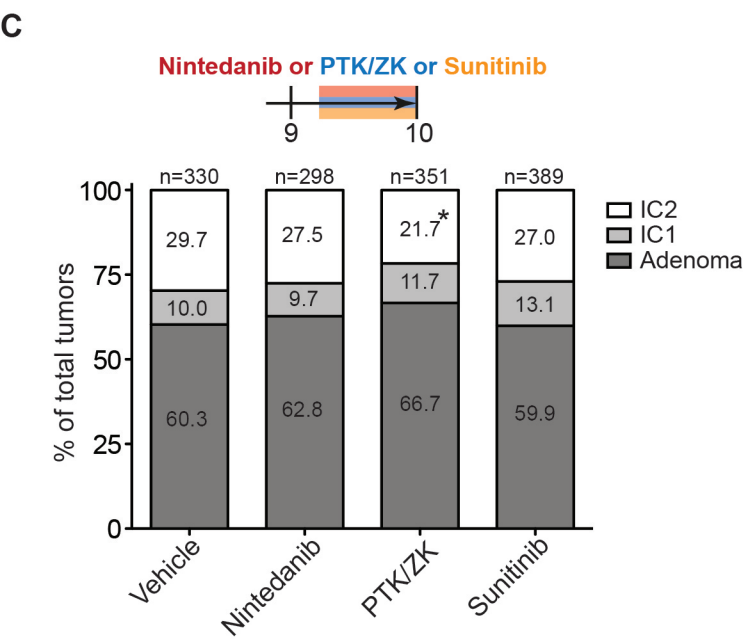

Supplemental Figure S5

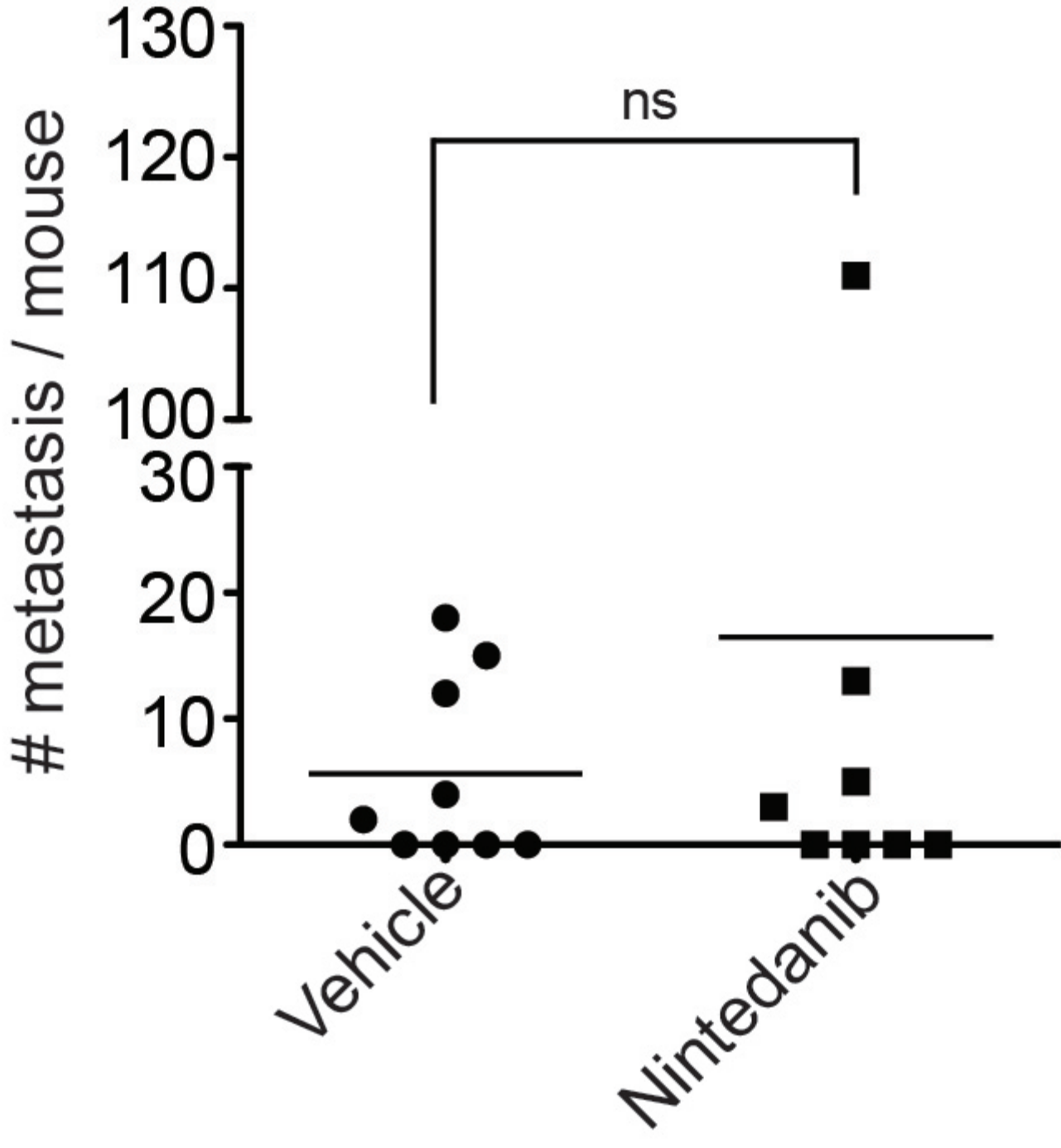

Supplemental Figure S6

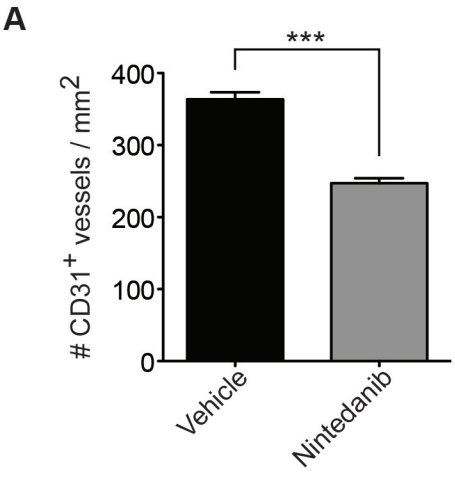

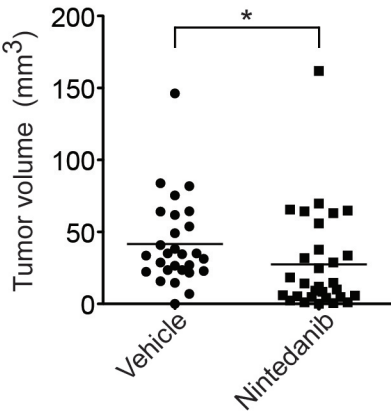

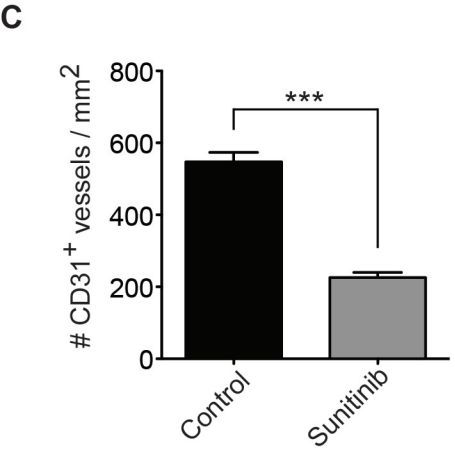

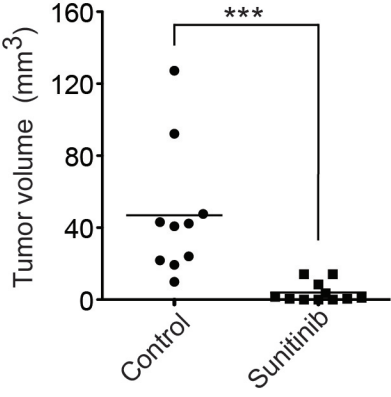

Supplemental Figure S7